Eur. Phys. J. C (2025) 85:494
https://doi.org/10.1140/epjc/s10052-025-14231-9

THE EUROPEAN PHYSICAL JOURNAL C

Regular Article - Theoretical Physics

Circular orbits and collisions of particles with magnetic dipole moment around magnetized Bocharova–Bronnikov–Melnikov–Bekenstein black holes

Nuriddin Kurbonov[1,2,a], **Ashfaque H. Bokhari**[3,b], **Javlon Rayimbaev**[4,c], **Bobomurat Ahmedov**[5,d]

[1] Institute for Advanced Studies, New Uzbekistan University, Movarounnahr str. 1, Tashkent 100000, Uzbekistan
[2] Shahrisabz State Pedagogical Institute, Shahrisabz Str. 10, Shahrisabz 181301, Uzbekistan
[3] Mathematics Department, College of Computing and Mathematics, King Fahd University of Petroleum and Minerals (KFUPM), P.O. Box 31261, Dhahran 31262, Saudi Arabia
[4] Urgench State University, Kh. Alimdjan str. 14, Urgench 220100, Uzbekistan
[5] Institute of Theoretical Physics, National University of Uzbekistan, Tashkent 100174, Uzbekistan

Received: 10 March 2025 / Accepted: 24 April 2025

Abstract In this study, we investigate the motion of magnetized particles around a Bocharova–Bronnikov–Melnikov–Bekenstein (BBMB) black hole in an external magnetic field, emphasizing the effects of an external magnetic field and a conformally coupled scalar field. We analyze the properties of circular orbits, the innermost stable circular orbit (ISCO), and the dynamics of high-energy particle collisions, focusing on the center-of-mass energy (CME) of colliding particles. We derive the equations governing the motion of magnetized particles in the BBMB spacetime and explore how the scalar coupling and the magnetic-dipole interaction parameters influence orbital stability and collision energetics. Our findings reveal that the ISCO radius is significantly modified by both scalar and magnetic interactions, leading to shifts in stability conditions and variations in the angular momentum requirements. The study also demonstrates that the critical angular momentum, which determines the transition between bound and unbound motion, is reduced compared to the Schwarzschild case due to the influence of the conformal scalar field. One key result is that the CME of colliding magnetized particles can be significantly enhanced in the BBMB spacetime. Increasing magnetic interaction and a stronger attractive scalar field lead to higher CME values, making the BBMB black hole a potential site for high-energy astrophysical processes. This suggests that external magnetic fields and scalar interactions play a crucial role in energy extraction mechanisms and the formation of ultrarelativistic particles.

1 Introduction

The BBMB black hole is a unique solution of the Einstein field equations with a conformally coupled scalar field [1,2]. Unlike standard black holes, such as Schwarzschild and Reissner–Nordström (RN), the BBMB solution exhibits a nontrivial scalar field that influences the surrounding spacetime and affects the properties of test particles and radiation. One of the key features of this spacetime is the scalar hair, which represents a deviation from the no-hair theorem, a fundamental aspect of classical black hole physics [2]. The BBMB solution is particularly interesting because it can be viewed as an extremal limit of a charged black hole with an additional scalar charge. However, a notable issue is the divergence of the scalar field at the event horizon, which raises questions about its physical interpretation and stability. Some studies suggest that this divergence may indicate an instability under perturbations, while others propose that it could be resolved by considering modified gravity frameworks or additional boundary conditions [3,4].

Several studies have investigated the geodesic structure of BBMB black holes, analyzing the behavior of test particles, photons, and accretion disks in the close vicinity of such central objects. The motion of test particles around such black holes has been extensively studied, revealing deviations from Schwarzschild-like orbits due to the influence of the conformal scalar field [5]. The ISCOs, which play a crucial role in

[a] e-mail: 1995krun@gmail.com
[b] e-mail: abokhari@kfupm.edu.sa
[c] e-mail: javlon@astrin.uz (corresponding author)
[d] e-mail: ahmedov@astrin.uz

Published online: 06 May 2025

accretion physics and QPO analysis, are significantly modified in the presence of the scalar field. This affects the energy efficiency of the accretion disks and changes the electromagnetic signatures observed from black hole accretion systems [6,7]. In addition, the behavior of massive and massless scalar fields represented by the covariant Klein–Gordon equation with BBMB spacetime is explored in Ref. [8]. The effect of the scalar field on shadow and quasinormal modes has also been explored, showing that deviations from general relativistic predictions could serve as a test for alternative theories of gravity [9,10].

The thermodynamic properties of BBMB black holes have also been another area of active research, particularly in the context of black hole entropy and temperature [11,12]. Unlike classical black holes, the presence of a scalar field requires modifications to the first law of thermodynamics, leading to corrections in entropy and Hawking radiation emission spectra. Some studies suggest that the BBMB solution may suffer from thermodynamic instability, while others propose ways to regularize its behavior by introducing additional constraints on the scalar field [8].

Thin and ionized accretion disks around a BBMB black hole have been studied in Ref. [13] using the Novikov–Thorne model, considering the presence of an external asymptotically uniform magnetic field. The motion of charged particles near a weakly magnetized black hole was analyzed, and it was found that the magnetic field shifts the marginally stable circular orbit closer to the event horizon. The four-acceleration of charged particles is also derived, and the radiation intensity emitted by their relativistic motion is calculated, showing that the magnetic field enhances high-energy emission.

Geodesic motion in the BBMB spacetime was analyzed to explore its gravitational features. The thermodynamic properties were examined in Ref. [14], revealing that the Hawking temperature vanishes. The motion of both massive and massless particles was studied, with characteristic radii and energy efficiency up to 8% determined for massive particles. The capture cross sections, pericentric precession, light deflection, and gravitational lensing were derived, showing that gravitational effects in the BBMB spacetime are weaker than those in the Schwarzschild case.

In addition to theoretical studies, potential astrophysical applications of BBMB black holes have also been explored in the literature, particularly in black hole mergers, accretion physics, and high-energy phenomena. The interaction of BBMB black holes with matter and radiation is a key area where deviations from general relativity can be tested. For example, the dynamics of hotspot motion in accretion disks around BBMB black holes exhibit deviations from standard models, which can be used for very-long-baseline interferometry (VLBI) observations [6]. The study of high-energy particle collisions near the BBMB black hole horizon has revealed that the Banados–Silk–West (BSW) process is significantly enhanced in this spacetime, leading to the possibility of producing ultrahigh-energy cosmic rays in astrophysical environments [5]. Additionally, gravitational wave signatures from perturbed BBMB black holes exhibit modifications in their quasinormal mode spectra, providing an avenue for testing alternative gravity models using gravitational wave observatories such as LIGO, Virgo, and LISA [15,16]. The role of BBMB black holes in braneworld gravity and teleparallel gravity has also been explored, demonstrating that modifications to general relativity can lead to novel predictions for astrophysical observations [17]. Future studies using next-generation X-ray and radio telescopes could further refine our understanding of BBMB black holes, potentially distinguishing them from Kerr black holes.

The study of magnetized particle motion around black holes has been an important area of research, which provides an interplay between gravitational and electromagnetic forces in extreme astrophysical environments. In the foundational work of Petterson (1974), this field has evolved significantly and explored the influence of magnetic fields on accretion disks around rotating black holes, highlighting the perturbations induced by misaligned magnetic fields on disk structures [18]. De Felice and Sorge (2003) further extended this study by analyzing the dynamics of magnetized particles near a Schwarzschild black hole immersed in a strong, asymptotically uniform magnetic field. Their study demonstrates that such magnetic fields substantially modify the effective potential that governs particle motion, leading to changes in stable circular orbits and the emergence of novel equilibrium configurations [19]. Building upon these insights, subsequent research has led to various black hole spacetimes and magnetic field configurations to understand their collective impact on magnetized particle trajectories. In recent years, the focus has expanded to encompass the combined effects of particle spin and magnetic dipole moments in black hole spacetimes. Utilizing the Mathisson–Papapetrou–Dixon equations, an interplay between gravitational and electromagnetic interactions has been demonstrated [20]. These studies underscore the necessity of incorporating both gravitational and electromagnetic interactions in modeling particle dynamics around black holes, offering a more comprehensive framework for exploring high-energy astrophysical processes.

The study of energetic processes around black holes, particularly those involving collisions of particles, has attracted significant attention due to its implications in high-energy astrophysics and potential energy extraction mechanisms. The collisional Penrose process, first proposed by Penrose in 1969, uses the ergosphere of a rotating black hole to extract rotational energy through particle interactions [21]. Subsequent studies have expanded this concept, notably with the mechanism BSW, which demonstrates that the CME of

two colliding particles near an extremal Kerr black hole can become arbitrarily large if one particle has a critical angular momentum [22]. This process has been extensively analyzed in various black hole spacetimes, including Kerr and RN, revealing that fine-tuning particle trajectories enhances efficiency [23,24]. For particles with magnetic dipoles, the dynamics become more intricate due to interactions with external magnetic fields, often present around astrophysical black holes due to accretion disks [25,26]. Studies, such as those by Bejger et al. and Leiderschneider et al., have numerically and analytically explored how these collisions amplify CME, with efficiencies reaching up to 14 times the initial energy under idealized conditions [27,28]. A magnetic dipole moment introduces additional forces, altering the effective potential and ISCOs, as demonstrated in studies of magnetized particles around Kerr black holes [29]. These investigations highlight that magnetic interactions can enhance or suppress energy extraction depending on the field strength and orientation [30]. Furthermore, as explored in braneworld black hole scenarios, collisions involving spinning particles show increased efficiencies with decreasing charge parameters, exceeding Kerr limits in some cases [31]. Numerical simulations like those by East and Pretorius have revisited high-energy head-on collisions, estimating gravitational radiation and confirming that black hole formation thresholds are lower than previously thought [32]. The interplay between gravitational lensing and magnetic effects in these collisions has been shown to concentrate energy, facilitating black hole formation [33]. In the context of supermassive black holes, where Hawking radiation is negligible, astrophysical mechanisms like cosmic microwave background interactions limit spin. Yet, dark matter annihilation via the Penrose process remains a promising avenue [34]. These studies underscore the complexity of energetic processes around black holes, with CME as a critical metric for understanding particle dynamics and energy release.

The CME of particles with magnetic dipoles in black hole spacetimes provides a unique lens into the physics of high-energy collisions and their astrophysical implications. Analytical and numerical studies have shown that the CME can diverge near the horizons of extremal black holes, particularly when magnetic dipole interactions are considered [35–38]. For instance, the circular motion of magnetized and charged particles around Kerr black holes immersed in external magnetic fields find that the CME increases with magnetic coupling parameters, impacting ISCO radii and energy efficiency [39]. Magnetized particle dynamics and collision have been studied and shown that magnetic dipoles enhance CME near rotating black holes in Horndeski gravity [40]. The inclusion of magnetic dipoles introduces a Lorentz-like force, modifying geodesic motion and amplifying energy release in collisions, as seen in studies of Schwarzschild and Kerr spacetime geometries [30,38]. The circular motion and collisions of particles in the ergoregion of a rotating and twisting charged black holes are studied [41]. Numerical calculations, such as those by Williams, have expanded the parameter space, incorporating reactions like Compton scattering and pair production, revealing that magnetic fields can modulate energy spectra [42]. In rotating spacetimes, the ergosphere facilitates negative energy states, allowing the Penrose process to extract rotational energy, with magnetic dipoles further boosting this effect [43]. Patel et al. demonstrated that electromagnetic extensions of the Penrose process in Kerr black holes with ambient magnetic fields lead to higher CMEs, particularly for near-horizon collisions [44]. Conversely, gravitational radiation and backreaction can limit efficiency, as noted in non-linear collisional Penrose studies [45]. For non-Kerr geometries, such as those in Rastall gravity, the CME of magnetized particles increases with electric and magnetic charges yet remains finite unless extremal conditions are met [46]. High-energy collision belts around accelerating black holes show that CME depends on the acceleration of parameters, with magnetic dipoles altering collision zones [47]. The astrophysical relevance is evident in studies linking these processes to jet formation via the Blandford–Znajek mechanism, where magnetic fields play a pivotal role [25].

In this study, we use the signature $(-,+,+,+)$ to represent the spacetime and unit system, with the unit system $G = c = 1$. However, for an astrophysical application, we explicitly include the speed of light in our formulations. The range of Latin indices spans from 1 to 3, whereas Greek indices range from 0 to 3.

2 Magnetization of BBMB black holes

The action of Einstein's gravity coupled to a conformally invariant scalar field Φ is given by:

$$S = \int d^4x\sqrt{-g}\left[\frac{R}{16\pi G} - \frac{1}{2}g^{\mu\nu}\Phi_{,\mu}\Phi_{,\nu} - \frac{R}{12}\Phi^2\right], \quad (1)$$

where R is the Ricci scalar, $g = \det(g_{\mu\nu})$ is the determinant of the metric tensor, the scalar field Φ is conformally coupled to gravity via the term $\frac{1}{12}R\Phi^2$. The stress-energy tensor for the conformally coupled scalar field is:

$$T_{\mu\nu} = \Phi_{,\mu}\Phi_{,\nu} - \frac{1}{2}g_{\mu\nu}g^{\alpha\beta}\Phi_{,\alpha}\Phi_{,\beta} + \frac{1}{6}\left(g_{\mu\nu}\Box - \nabla_\mu\nabla_\nu + G_{\mu\nu}\right)\Phi^2. \quad (2)$$

The black hole solution can be obtained for the conformal scalar field $\Phi(r) = M/(r-M)$ in the following form [2]:

$$ds^2 = -f(r)dt^2 + \frac{dr^2}{f(r)}dr^2 + r^2\left(d\theta^2 + \sin^2\theta d\phi^2\right), \quad (3)$$

where $f(r) = \left(1 - \frac{M}{r}\right)^2$. We assume that the black hole is immersed in an external magnetic field that is asymptotically uniform and weak enough that it does not affect the black hole's geometry. The Maxwell equations,

$$\frac{1}{\sqrt{-g}}\partial_\mu(\sqrt{-g}F^{\mu\nu}) = 0, \tag{4}$$

where $F_{\mu\nu} = A_{\nu,\mu} - A_{\mu,\nu}$ is electromagnetic field (antisymmetric) tensor. The expression for the vector potential in the standard form is,

$$A_\phi = \frac{B}{2}r^2\psi(r)\sin^2\theta, \tag{5}$$

where B_0 represents the asymptotic value of the magnetic field. In the provided context, $\psi(r)$ is a radial function that is determined as a solution to the Maxwell equation, (4).

The Maxwell's equations are:

$$\partial_r\left(r^2\sin\theta F^{r\phi}\right) + \partial_\theta\left(r^2\sin\theta F^{\theta\phi}\right) = 0, \tag{6}$$

$$\partial_r\left[r^2\sin\theta g^{rr}g^{\phi\phi}F_{r\phi}\right] + \partial_\theta\left[g^{\theta\theta}g^{\phi\phi}r^2\sin\theta F_{\theta\phi}\right] = 0. \tag{7}$$

Since this must vanish separately, we focus on the equation for the radial component only:

$$\frac{\partial}{\partial r}\left[r^2\left(1 - \frac{M}{r}\right)^2\left(2r\psi + r^2\frac{\partial\psi}{\partial r}\right)\right] - 2\psi = 0. \tag{8}$$

Solving this differential equation, we get the general solution given by,

$$\psi(r) = 1 - \frac{M^2}{r^2}. \tag{9}$$

Accordingly, the final solution for A_ϕ becomes:

$$A_\phi = \frac{B}{2}r^2\left(1 - \frac{M^2}{r^2}\right)\sin^2\theta. \tag{10}$$

The strength of the external magnetic field in the curved spacetime background is calculated using the expression

$$B^\alpha = \frac{1}{2}\eta^{\alpha\beta\sigma\mu}F_{\beta\sigma}w_\mu \tag{11}$$

where w_μ is the four-velocity of an observer, $F_{\beta\sigma}$ is electromagnetic field tensor. The symbol $\eta_{\alpha\beta\sigma\gamma}$ is the pseudo-tensorial representation of the Levi-Civita symbol, denoted by $\epsilon_{\alpha\beta\sigma\gamma}$ and is characterized by the following form:

$$\eta_{\alpha\beta\sigma\gamma} = \sqrt{-g}\epsilon_{\alpha\beta\sigma\gamma} \qquad \eta^{\alpha\beta\sigma\gamma} = -\frac{1}{\sqrt{-g}}\epsilon^{\alpha\beta\sigma\gamma}. \tag{12}$$

The magnetic field's components in an orthonormal coordinate system can be represented by utilizing the electromagnetic field tensor in the following form:

$$B^{\hat{i}} = \frac{1}{2}\epsilon_{ijk}\sqrt{g_{jj}g_{kk}}F^{jk} = \frac{1}{2}\epsilon_{ijk}\sqrt{g^{jj}g^{kk}}F_{jk}. \tag{13}$$

Consequently, the non-zero components of the external magnetic field, as observed by a proper observer with the four-velocity $w^\mu_{\text{proper}} = (1/\sqrt{-g_{tt}}, 0, 0, 0)$, can be obtained as,

$$B^{\hat{r}} = B\left(1 - \frac{M^2}{r^2}\right)\cos\theta \quad B^{\hat{\theta}} = B\left(1 - \frac{M}{r}\right)\sin\theta. \tag{14}$$

3 Motion of Magnetized particles

The Hamilton-Jacobi equation that takes into account both interactions between the magnetized particles with conformal scalar and magnetic fields has the form

$$g^{\mu\nu}\frac{\partial S}{\partial x^\mu}\frac{\partial S}{\partial x^\nu} = -m^2\left(1 + g_s\Phi(r)\right)^2\left(1 - \frac{\mathcal{U}}{2m}\right)^2, \tag{15}$$

where g_s is the conformal scalar field coupling parameter responsible for interaction between the scalar field and magnetized particles. The scalar product $\mathcal{U} = D^{\mu\nu}F_{\mu\nu}$ corresponds to the magnetic interaction between the field and the particles, with $D^{\mu\nu}$ representing the polarization tensor.

The Lagrangian of the magnetized particles in curved spacetime has a form [48],

$$\mathcal{L} = \frac{1}{2}\left(m(1 + g_s\Phi(r)) + \mathcal{U}\right)g_{\mu\nu}u^\mu u^\nu - \frac{1}{2}\mathcal{U}. \tag{16}$$

The interaction term has been calculated in Refs. [49–60] as $\mathcal{U} = \mu_{\hat{\alpha}}B^{\hat{\alpha}}$. In our further analyses, we consider the magnetic dipole of the particles to be perpendicular to the equatorial plane (so it has components $\mu^{\hat{\alpha}} = (0, 0, \mu, 0)$) and restricted the particle's motion in that plane. Thus, the interaction term takes $\mathcal{U} = \mu_{\hat{\theta}}B^{\hat{\theta}} = \mu B\sqrt{f(r)}$.

One may easily find integrals of motion of magnetized particles ($p_\phi = L = mu^\phi$ and $p_t = -E = mu^t$ denoting the total angular momentum and total energy of the particle, respectively) using the above Lagrangian in the following form,

$$\dot{t} = \frac{\mathcal{E}}{-g_{tt}\left(1 + g_s\Phi(r) + \beta\sqrt{f(r)}\right)}, \tag{17}$$

$$\dot{\phi} = \frac{\mathcal{L}}{g_{\phi\phi}\left(1 + g_s\Phi(r) + \beta\sqrt{f(r)}\right)}, \tag{18}$$

where $\beta = \mu B/m$ is the magnetic interaction parameter. Compact objects with dipole magnetic moment, in particular, neutron stars (NSs) and white dwarfs (WDs) can be treated as a magnetized test particle, orbiting supermassive or intermediate-mass black holes ($M_{\text{WD}} < M_{\text{NS}} \ll M_{\text{BH}}$) immersed in an external magnetic field. Magnetized NSs and WDs with magnetic dipole moment $\mu_{\text{NS}} = (1/2)B_{\text{NS}}R^3_{\text{NS}}$ and $\mu_{\text{WD}} = (1/2)B_{\text{WD}}R^3_{\text{WD}}$, respectively. The magnetic coupling parameter β is estimated using obser-

vational parameters:

$$\left\{\beta_{\rm NS}, \beta_{\rm WD}\right\} \simeq \frac{44}{10^4}\frac{B_1}{M_1}\left\{B_{12}R_6^3, B_4R_9^3\right\} \tag{19}$$

where $B_{12} = B_{\rm NS}/(10^{12}{\rm G})$, $B_4 = B_{\rm WD}/(10^4{\rm G})$ and $B_1 = B_0/(10\,{\rm G})$ are dimensionless surface magnetic fields of the NS and WD normalized to 10^{12}G, 10^4G and 10G, respectively, $R_6 = R_{\rm NS}/(10^6{\rm cm})$ and $R_9 = R_{\rm WD}/(10^9{\rm cm})$ are normalized values of the NS and WD radii to 10 km and 10^4 km, respectively, and the masses of the stars are normalized to the solar mass, $M_1 = m_{\rm (NS/WD)}/M_\odot$.

The Hamilton-Jacobi action for the motion of magnetized particles in the equatorial plane ($\theta = \pi/2$) can be separated as follows:

$$S = -Et + L\phi + S_r(r). \tag{20}$$

Using the Hamilton-Jacobi equation (15), we can obtain the equation of radial motion of the magnetized particles given by,

$$g^{rr}\left(\frac{\partial S_r}{\partial r}\right)^2 + g^{tt}\mathcal{E}^2 + g^{\phi\phi}\mathcal{L}^2 = (1+g_s\Phi(r))^2\left(1-\beta\sqrt{f(r)}\right)^2. \tag{21}$$

After some lengthy calculations, we obtain the following:

$$V_{\rm eff} = f(r)\left[(1+g_s\Phi(r))^2\left(1-\beta\sqrt{f(r)}\right)^2 + \frac{\mathcal{L}^2}{r^2}\right]. \tag{22}$$

Figure 1 illustrates the radial dependence of the effective potential V_{eff} for magnetized particles orbiting a BBMB black hole. The potential is plotted as a function of the dimensionless radial coordinate r/M and for different values of the scalar coupling parameter g_s and the magnetic dipole interaction parameter β, with a fixed angular momentum $\mathcal{L} = 4\,M$ typical for circular orbits. The solid curve represents the case with $g_s = \beta = 0$ (no scalar or magnetic interactions), showing a baseline potential dominated by gravitational effects. The dashed curve corresponds to $g_s = 0.1$ and $\beta = 0$, highlighting the enhancement of the potential barrier due to the conformal scalar field $\Phi = M/(r-M)$. The dotted curve, with $g_s = 0$ and $\beta = 0.2$, demonstrates the modification induced by the magnetic dipole moment, reducing the potential near the horizon due to the term which is proportional to $1-\beta\sqrt{f(r)}$. The combined effect ($g_s = 0.1$, $\beta = 0.2$) reveals a complex interaction, changing the positions of the potential's minima and maxima, corresponding to stable and unstable circular orbits. The vertical line at $r = M$ marks the event horizon, beyond which the potential diverges due to the singularity of the scalar field potential $\Phi(r) = M/(r-M)$. This figure underscores how scalar and magnetic interactions alter the dynamics of magnetized particles, influencing the innermost stable circular orbit (ISCO) and collision energetics near the BBMB black hole.

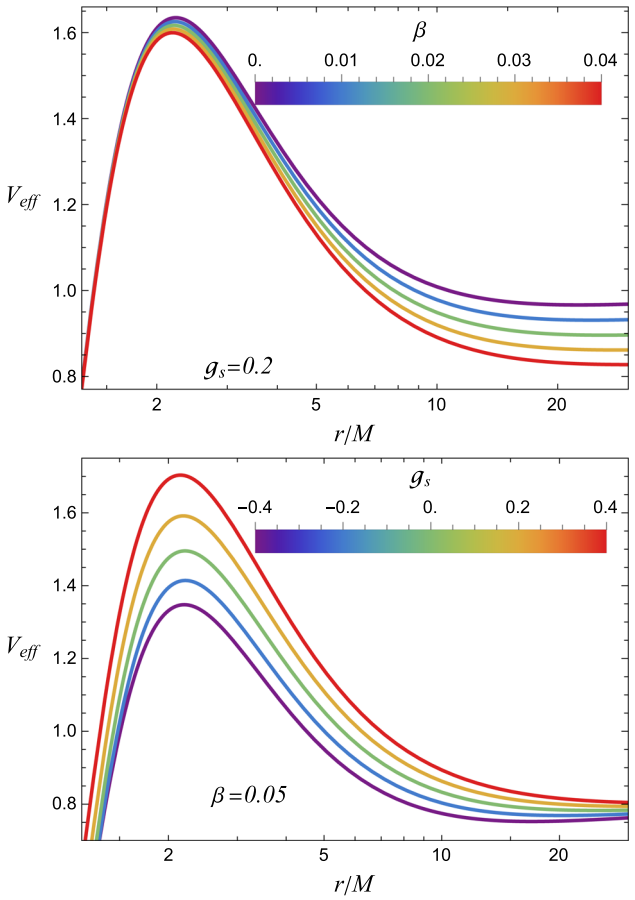

Fig. 1 Radial dependence of the effective potential for magnetized particles around BBMB BHs

3.1 Circular orbits of magnetized particles

The minima of the effective potential correspond to stable circular orbits, where a small radial perturbation results in bounded oscillations around an equilibrium position. The orbits where the affective potential reaches a maximum indicate unstable circular orbits. A slight perturbation can cause the particle to fall into the central object or escape to infinity. The steepness and shape of the potential provide insights into the gravitational well and the forces which govern orbital motion. For circular orbits, the following conditions must be satisfied:

$$\frac{dV_{\rm eff}}{dr} = 0, \quad \frac{d^2V_{\rm eff}}{dr^2} > 0. \tag{23}$$

From $\partial_r V_{\rm eff} = 0$, we derive the angular momentum $\mathcal{L}$ and energy $\mathcal{E}$ for circular orbits.

$$\mathcal{L}^2 = \frac{Mr\left(1-\beta(1-\frac{M}{r})\right)(M(g_s-1)+r)}{(r-M)\left(2M^2-3Mr+r^2\right)}$$

$$\times\Big[g_s\left\{2\beta M^2+r^2\left(\beta+1-\frac{M}{r}\right)-3\beta Mr\right\} -2\beta(M-r)^2-r(M-r)\Big] \tag{24}$$

and

$$\mathcal{E}^2=\left(1-\frac{M}{r}\right)^2\left\{1-\left(1+\beta\left(1-\frac{M}{r}\right)\right)^2\left(1+\frac{Mg_s}{r-M}\right)^2 -\frac{M((\beta-1)r-\beta M)\,(Mg_s-M+r)}{r^2\left(2M^2-3Mr+r^2\right)} \times\left(g_s(-2\beta M+\beta r+r)+2\beta M-2\beta r+r\right)\right\}. \tag{25}$$

Figure 2 shows the relationships between energy $\mathcal{E}$ and angular momentum $\mathcal{L}$ (top panels) and radial dependence of energy (bottom panels) for particles with magnetic dipole moment in circular orbits around a magnetized BBMB black hole. This figure also examines magnetized particles' energetics and orbital dynamics in the BBMB spacetime, characterized by the metric function $f(r)=(1-M/r)^2$ and scalar field, with the event horizon at $r=M$. The top panels display the energy $\mathcal{E}$(normalized by particle mass m) as a function of angular momentum $\mathcal{L}/M$ for circular orbits in the equatorial plane ($\theta=\pi/2$), derived from the Hamilton-Jacobi equation and effective potential V_{eff}. Plots in the bottom panels demonstrate the dependence of $\mathcal{E}$ versus radial distance r/M for these orbits, highlighting the radial variation influenced by gravitational, scalar, and magnetic interactions.

The left top panel shows $\mathcal{E}$ versus $\mathcal{L}/M$ for varying scalar coupling g_s with fixed magnetic dipole parameter $\beta=0$. The solid curve ($g_s=0$) represents the baseline BBMB case, where the energy exhibits a minimum at $\mathcal{L}/M\simeq 4$, corresponding to the innermost stable circular orbit (ISCO) without scalar effects. As the scalar field interaction increases (dashed and dotted curves), the conformal scalar field amplifies the potential term $(1+g_s\Phi(r))^2$, shifting the minimum energy to higher angular momentum and reducing the ISCO radius, reflecting stronger binding due to scalar-gravity coupling. The right top panel varies β with $g_s=0$. The magnetic dipole interaction via $(1-\beta\sqrt{f(r)})$ lowers the energy at fixed values of the angular momentum, as the Lorentz-like force opposes gravitational attraction, pushing the ISCO outward and flattening the curve near the horizon. The energy minimum broadens for large values of β, indicating a wider range of stable angular momentum. These graphs reveal critical values $\mathcal{L}$ where $\partial_r V_{eff}=0$ (circular orbit condition) and $\partial_{rr}V_{eff}>0$ (stability), modified by the scalar and magnetic interactions. The left bottom panel plots illustrate $\mathcal{E}(r)$ for circular orbits with fixed $\mathcal{L}/M=4$, varying g_s for β=0. The solid curve (g_s=0) shows a monotonic decrease in $\mathcal{E}$ toward $r=M$, with a minimum near the ISCO ($r\simeq 1.5M$), beyond which orbits become unstable. With increasing g_s, the scalar field's divergence near $r=M$ steepens the potential, reducing $\mathcal{E}$ at smaller radii and shifting the ISCO inward, consistent with enhanced gravitational attraction. The right bottom panel varies β (for example, β = 0,0.1,0.3, g_s = 0) for the fixed value of $\mathcal{L}$. The magnetic dipole reduces $\mathcal{E}$ near the horizon, as the term $1-\beta\sqrt{f(r)}$ weakens the effective binding energy, pushing the ISCO to larger r (from $1.5M$ to $2M$ as β rises). The vertical dashed line at $r=M$ marks the horizon, where $\mathcal{E}$ approaches a finite value for stable orbits but diverges for plunging trajectories due to $\Phi(r)$.

The top panels illustrate how g_s tightens orbital stability, requiring a higher value of $\mathcal{L}$ to counter the scalar field, while β relaxes this constraint, enabling stable orbits at lower energies. The bottom panels show the radial sensitivity of $\mathcal{E}$, with g_s enhancing near-horizon binding and β counteracting it, affecting collision energetics (refer to section V). These dependencies highlight the BBMB black hole's unique interplay of conformal scalar and magnetic effects which are distinct from Kerr or Schwarzschild spacetimes. This has implications for energy extraction and particle acceleration near the horizon.

4 ISCO of magnetized particles

The second derivative of the effective potential determines the stability of circular orbits: $\partial_r^2 V_{\rm eff}>0$.

When this condition is not met, unstable circular orbits occur, indicating that the particle will spiral inward toward the BH or outward into escape trajectories. Circular orbits occur at radii where the radial component of the particle's motion vanishes. Mathematically, this is given by: $\partial_r V_{\rm eff}=0$. This condition provides the radius of the circular orbit, r_c, as a function of the central object's parameters, including environments, such as the BH mass and the coupling parameters [61]. By numerically solving the conditions for $\partial_r V_{\rm eff}=0$ and $\partial_r^2 V_{\rm eff}>0$, one can map out the stability regions in the parameter space. The ISCO is determined by solving the following equations simultaneously:

$$\partial_r V_{\rm eff}=0,\quad \partial_r^2 V_{\rm eff}=0. \tag{26}$$

Figure 3 illustrates the dependence of the ISCO radius $r_{\rm ISCO}$, along with the corresponding angular momentum $\mathcal{L}_{\rm ISCO}$ and energy $\mathcal{E}_{\rm ISCO}$ for magnetized particles around a BBMB black hole. It highlights how the combined effects of an external magnetic field and a conformally coupled scalar field modify the ISCO and its associated parameters. The left panels show variations with the magnetic coupling parameter β, while the right panels display variations with the scalar coupling parameter g_s. The top row of the figure depicts the dependence of the ISCO radius $r_{\rm ISCO}$ on β (left) and g_s (right): as β increases from 0 to 0.04, $r_{\rm ISCO}$ shifts outward. This is due to the additional Lorentz force resulting from

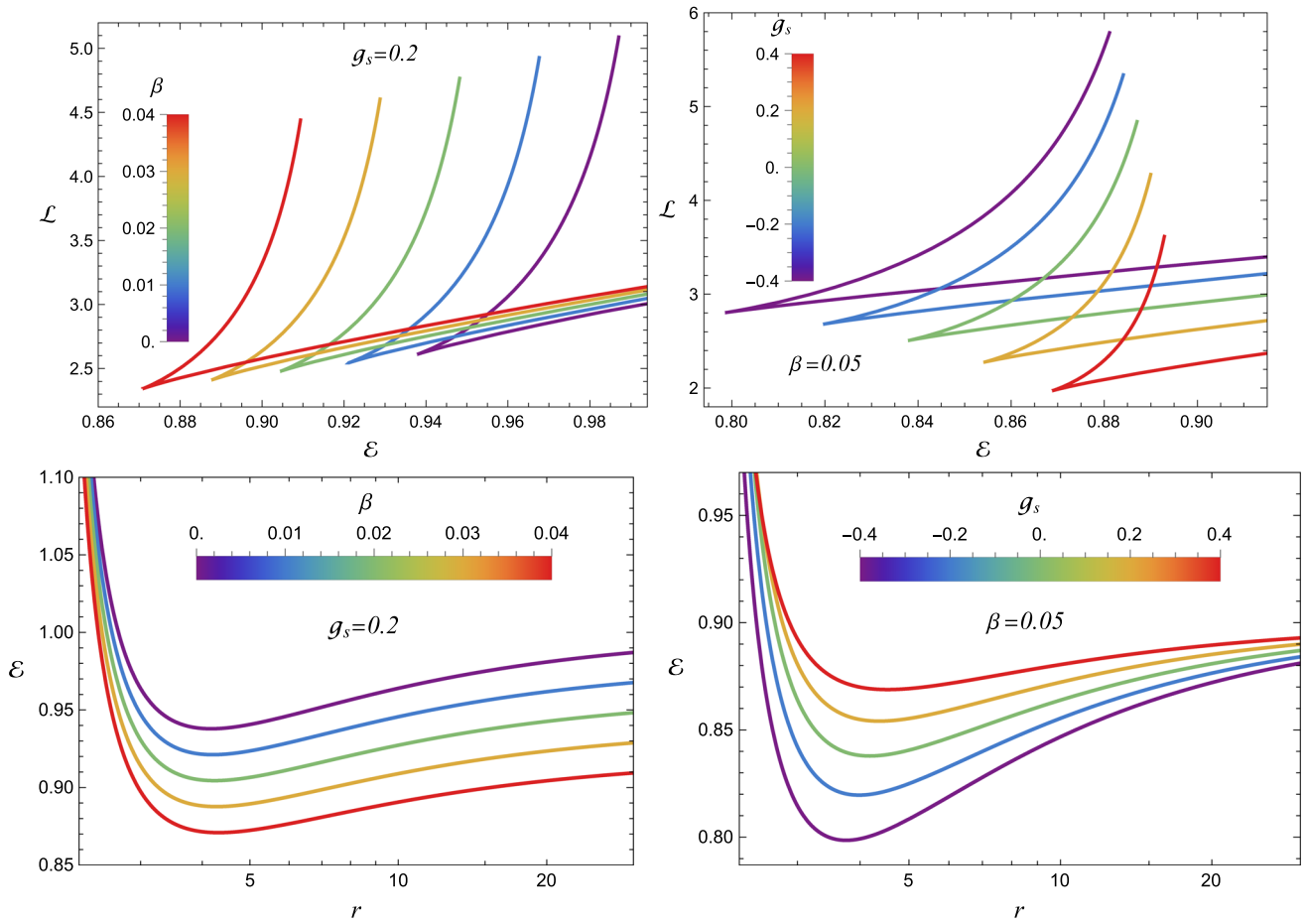

Fig. 2 The relationships between the energy $\mathcal{E}$ and angular momentum $\mathcal{L}$ (top panels) and radial dependence of energy (bottom panels) of particles with magnetic dipole moment at circular orbits around magnetized BBMB black hole

the interaction between the external magnetic field and the particle's dipole moment. A positive g_s enhances gravitational attraction, pulling the ISCO inward, while a negative g_s weakens the gravitational potential, causing the ISCO to shift outward. The middle row illustrates the variation of the angular momentum required for ISCO: as β increases, $\mathcal{L}_{\rm ISCO}$ also increases. The added magnetic interaction necessitates higher angular momentum to counteract the magnetic repulsion. For positive g_s, a stronger gravitational attraction requires more significant angular momentum for stability, whereas negative g_s leads to a decrease in $\mathcal{L}_{\rm ISCO}$. The bottom row of Fig. 3 presents the energy $\mathcal{E}_{\rm ISCO}$ at ISCO: as β increases, there is a slight increase in $\mathcal{E}_{\rm ISCO}$, indicating that particles need more energy to reach and maintain stable circular orbits. A positive g_s increases the gravitational potential depth, leading to higher energy requirements, whereas a negative g_s lowers $\mathcal{E}_{\rm ISCO}$. These findings carry significant astrophysical implications. Since the ISCO establishes the inner edge of the accretion disk, the observed luminosity and spectral features of black hole systems will be influenced by β and g_s. If $r_{\rm ISCO}$ shifts outward due to magnetic interactions, the structure of the accretion disk will become less compact. Variations in $\mathcal{E}_{\rm ISCO}$ affect particle acceleration and the formation of relativistic jets. The influence of the scalar field in altering ISCO properties can serve as an observational test for deviations from general relativity. These modifications directly impact astrophysical observables, including the properties of black hole accretion disks and high-energy processes near compact objects.

5 Magnetized particle collisions near BBMB BHs

The Penrose process effectively extracts rotational energy from a Kerr black hole by leveraging its ergosphere [21]. A particle entering the ergosphere splits into two parts, with one carrying negative energy falling into the black hole, reducing its angular momentum, while the other escapes with increased energy, potentially exceeding the initial energy by up to 20–30% [23]. This process has been extensively studied in rotating black hole spacetimes, with works by Blandford and Znajek extending it to electromagnetic extraction via

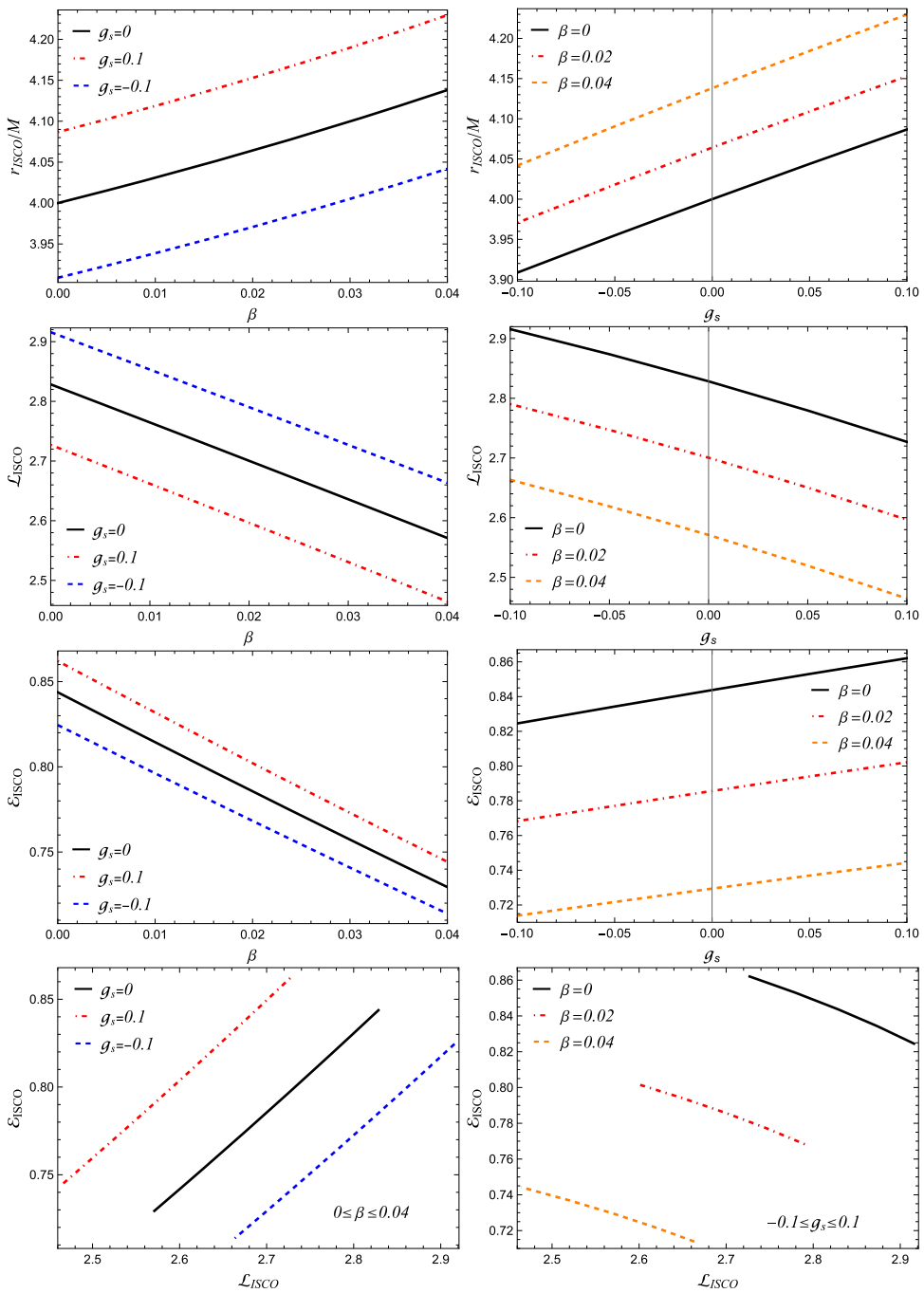

Fig. 3 Dependence of ISCO radius on β and g_s for magnetized Bocharova–Bronnikov–Melnikov–Bekenstein black hole

magnetic fields, crucial for powering astrophysical jets [25]. Magnetic fields can enhance energy extraction efficiency near Kerr black holes, particularly for particles with electric charges and/or dipole moments [62]. Numerical simulations by East and Pretorius demonstrate that high-energy collisions within the ergosphere can amplify energy release, though gravitational radiation limits efficiency [32]. The process's astrophysical relevance lies in its potential to explain jet formation in active galactic nuclei (AGN), with COM energies playing a key role in determining extraction rates [24]. However, challenges like particle fine-tuning and backreaction effects, as noted by Nakao, Okawa and Maeda, suggest that realistic efficiencies are lower than theoretical maxima [45]. These studies highlight the Penrose process's foundational impact on understanding black hole energetics, with COM energy serving as a critical parameter for assessing energy release in spacetimes of rotating objects.

The BSW mechanism, introduced in 2009, proposes that collisions near the horizon of an extremal Kerr black hole can achieve arbitrarily high CME in case one particle has critical angular momentum [22]. This process, distinct from the Penrose process, relies on the spacetime's geometry near

ISCOs, where relativistic effects amplify particle interactions [35]. BSW collisions in magnetized Kerr spacetimes have been potentially studied and found that interactions between magnetic fields and charged particles cause an increase in the CME, potentially reaching efficiencies orders of magnitude higher than standard astrophysical processes [39]. These studies have extended to spinning particles, showing efficiencies up to 14 times the initial energy under certain idealized conditions, though realistic astrophysical environments limit this [28]. The BSW mechanism's impact on astrophysics includes potential signatures in γ-ray bursts and ultra-high-energy cosmic rays as a model of particle acceleration near black holes [34]. However, constraints like gravitational radiation and horizon proximity suggest finite CME in non-extremal cases [63]. The mechanism's ability to probe quantum gravity effects near horizons underscores its theoretical significance. CME is a diagnostic for extreme astrophysical environments, influencing black hole accretion and jet dynamics.

Collisional processes around black holes, including head-on collisions and scattering, drive significant energy release, with CME determining astrophysical outcomes. Head-on collision cases near Kerr black holes can produce CME exceeding theoretical limits, potentially powering relativistic jets and gamma-ray emissions [27]. Collisions of magnetized and charged particles in Kerr and non-Kerr spacetimes show that magnetic dipole moments enhance the CME, affecting the ISCO radii and energy extraction efficiency [64]. Numerical simulations have revisited high-energy collisions, estimating gravitational wave emissions and black hole formation thresholds, revealing that CME influences merger dynamics [32,42]. These collisions, often occurring in dense accretion disks, contribute to black hole growth and jet launching as effects of magnetic fields on particle acceleration [65]. The astrophysical impact includes signatures in GW events detected by LIGO-Virgo, with CME shaping merger rates and spin distributions [66]. However, backreaction and energy loss via radiation are essential in constraining efficiency, particularly in magnetized spacetimes [30]. High CME near-horizons also probe fundamental physics, potentially revealing quantum gravity effects [67]. These studies underscore the role of CME in driving black hole energetics, jet formation, and observable astrophysical phenomena.

The probability of magnetized particles in astrophysical accretion disks around black holes is high, driven by the strong magnetic fields generated by dynamo processes and plasma dynamics. Magnetic fields, often on the order of $10^4 - 10^8$ Gauss, permeate accretion disks, influencing particle orbits and enhancing magnetized particle populations [65]. Particles with magnetic dipole moments, such as those in magnetized plasmas, are trapped or accelerated near black holes. This may increase their likelihood in dense disk regions due to Lorentz forces [62]. The energy of the magnetized Kerr black hole can be extracted through the Blandford–Znajek mechanism due to the magnetic field interaction and charged particles near the horizon [25]. Also, magnetic reconnection events within disks further boost magnetized particle densities, with probabilities peaking near the ISCO [68]. Observational evidence from X-ray binaries and AGN supports this, with magnetized particle signatures detected in disk emissions, suggesting a near-certain presence in such environments [34].

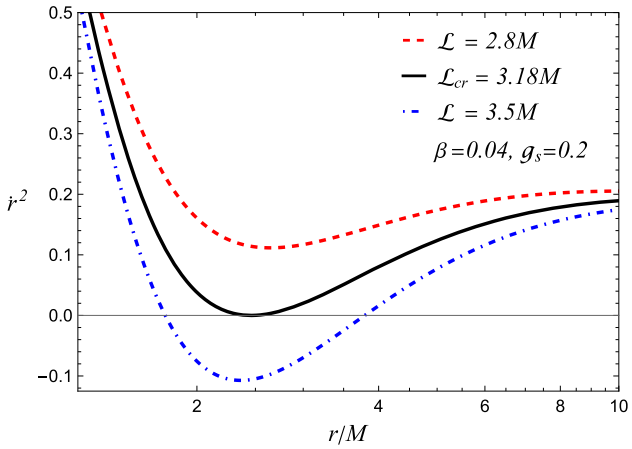

Fig. 4 Radial dependence of the square of radial velocity for different values of angular momentum

5.1 Critical angular momentum for magnetized particles orbiting black holes

The critical angular momentum $\mathcal{L}_{\rm cr}$ represents the threshold between bounded and unbounded motion. It determines whether a magnetized particle remains in a stable orbit, plunges into the black hole, or escapes to infinity. Understanding $\mathcal{L}_{\rm cr}$ is essential for:

- Predicting the structure and stability of accretion disks.
- Determining the efficiency of high-energy particle collisions.
- Exploring astrophysical processes such as energy extraction and jet formation.

It is crucial to acknowledge a captivating occurrence associated with angular momentum, a "critical value" necessary for approaching a black hole. Two conditions can determine the critical value of the angular momentum: (i) $\dot{r} = 0$ and (ii) $d\dot{r}/dr = 0$.

Figure 4 presents the radial dependence of the squared radial velocity $\dot{r}^2$ for magnetized particles orbiting a BBMB black hole in an external magnetic field. The figure examines different values of the particle's angular momentum $\mathcal{L}$,

highlighting how the scalar field and the magnetic dipole interaction modify particle dynamics.

In the Schwarzschild metric, the critical angular momentum required for a particle to be in an unstable circular orbit at the photon sphere ($r = 3M$) is $\mathcal{L}_{\rm cr} = 4M$ in Schwarzschild limit.

There are no stable circular orbits for particles with $\mathcal{L} < 4\,M$, and the particle will inevitably fall into the black hole. In contrast, in the BBMB spacetime, the conformally coupled scalar field and the external magnetic field significantly modify this behavior, affecting both the location and stability of circular orbits.

The figure illustrates how the radial velocity $\dot{r}^2$ varies with the radial coordinate r/M for different values of the angular momentum $\mathcal{L}$ under fixed values of the scalar coupling parameter $g_s = 0.2$ and the magnetic dipole interaction parameter $\beta = 0.04$. It is observed that when $\mathcal{L} < \mathcal{L}_{\rm cr}$, the radial velocity remains positive across all r, meaning the particle is in a plunging trajectory and will inevitably fall into the black hole. Near $\mathcal{L}_{\rm cr}$, there exists a turning point where $\dot{r}^2$ momentarily vanishes, corresponding to the location of an unstable circular orbit. In the case of $\mathcal{L} > \mathcal{L}_{\rm cr}$, the particle can remain in a stable orbit at some radial distance or even escape if perturbed.

Unlike the Schwarzschild case, where $\mathcal{L}_{\rm cr} = 4M$ at $r = 3M$, the BBMB case shows a shift in both the critical angular momentum and the radial location of unstable orbits. This shift occurs due to the presence of the scalar field enhancing gravitational attraction, reducing the required $\mathcal{L}_{\rm cr}$ and also the magnetic dipole interaction, which introduces an additional Lorentz-like force modifying particle motion.

These effects imply that particles in BBMB spacetime require less angular momentum to achieve a critical orbit than Schwarzschild spacetime, meaning that the black hole's gravitational potential is effectively deeper due to the influence of additional fields.

Figure 5 illustrates the dependence of the critical angular momentum $\mathcal{L}_{\rm cr}$ on the magnetic dipole interaction parameter β (top panel) and the scalar coupling parameter g_s (bottom panel) for magnetized particles moving in the vicinity of a BBMB black hole. The critical angular momentum plays a fundamental role in determining the stability of orbits of the particles and their possible trajectories under the combined influence of gravitational, scalar, and magnetic interactions.

The top panel of the figure shows the variation of $\mathcal{L}_{\rm cr}$ as a function of the magnetic dipole interaction parameter β while keeping the scalar coupling parameter fixed at $g_s = 0.0$. The results indicate that increasing β leads to an overall increase in $\mathcal{L}_{\rm cr}$, meaning that stronger magnetic dipole interactions require higher angular momentum for a particle to remain in orbit. The increase in $\mathcal{L}_{\rm cr}$ is more pronounced at smaller radii, where the magnetic force significantly alters the effective potential. The effect is due to the interaction between

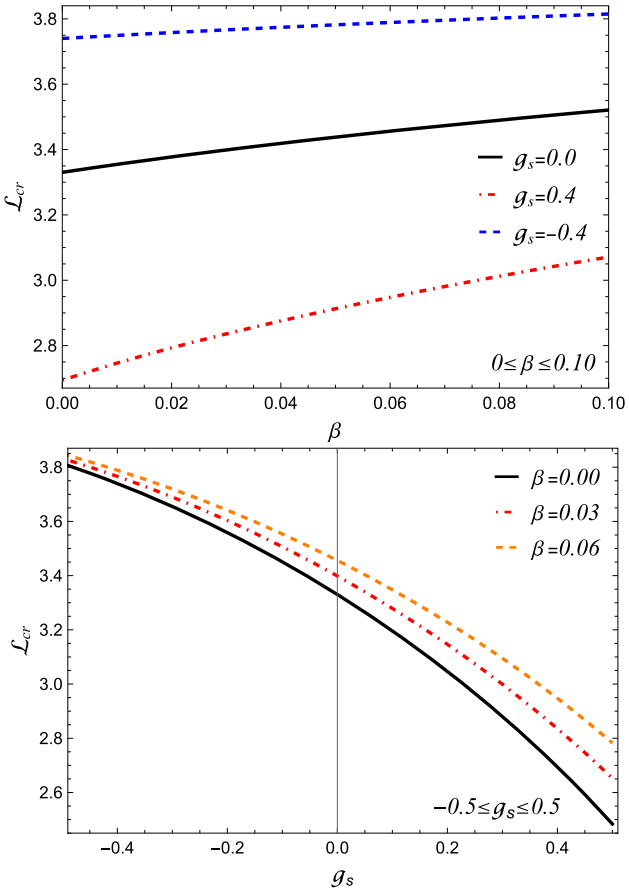

Fig. 5 Dependence of the critical angular momentum on β (top panels) and g_s (bottom panels)

the particle's magnetic dipole moment and the external magnetic field, which introduces an additional repulsive force that counteracts gravitational attraction, thereby shifting the stability conditions.

The bottom one examines the variation of $\mathcal{L}_{\rm cr}$ with the scalar coupling parameter g_s for a fixed value of the magnetic dipole parameter $\beta = 0.05$. One can observe from the results demonstrated that for the case $g_s < 0$ (repulsive scalar field), $\mathcal{L}_{\rm cr}$ decreases, meaning that particles require less angular momentum to maintain stable orbits. For $g_s = 0$, $\mathcal{L}_{\rm cr}$ follows the baseline BBMB behavior, providing a reference for comparison. For $g_s > 0$ (attractive scalar field), $\mathcal{L}_{\rm cr}$ increases significantly, suggesting that the additional gravitational pull strengthens orbital binding, requiring higher angular momentum to counterbalance the increased attraction.

This trend aligns with previous studies [69,70], where an attractive scalar field enhances the effective gravitational pull, leading to deeper potential wells and increasing the angular momentum required for stable orbits. These dependencies have essential implications for accretion disk stability, as the critical angular momentum determines the ISCO's

location and influences the accretion systems' luminosity and energy release. These findings are particularly relevant for understanding the evolution of magnetized plasmas around black holes and their role in high-energy astrophysical processes such as relativistic jets and energetic particle collisions.

5.2 Center of mass energy of colliding magnetized particles

Here, we study the center of mass of the two colliding magnetized particles involved in the collision for the center-of-mass frame of reference. We consider these particles to have initial energies $\mathcal{E}_1$ and $\mathcal{E}_2$ at infinity. We assume two particles of masses m_1 and m_2 moving along geodesics in the spacetime of the BBMB black hole. Then, their energy in the center of the mass frame can be determined as follows [71]:

$$\{E_{cm}, 0, 0, 0\} = p_1^{\mu} + p_2^{\mu}. \tag{27}$$

Using the four-momentum $p_1^{\alpha} = m_1 u_1^{\alpha}$ and $p_2^{\alpha} = m_2 u_2^{\alpha}$, which represent the moments of the two colliding particles, where u^{α} is the momentum per mass. It is straightforward to compute the square of the CME, as defined in Eq. (27). This calculation yields the desired result:

$$E_{cm}^2 = m_1^2 + m_2^2 - 2m_1 m_2 g_{\mu\nu} u^{\mu} u^{\nu} \tag{28}$$

or

$$\frac{E_{cm}^2}{m_1 m_2} = \frac{m_1}{m_2} + \frac{m_2}{m_1} - 2g_{\mu\nu} u_1^{\mu} u_2^{\nu}. \tag{29}$$

In case the masses of the colliding particles are $m_1 = Xm$ and $m_2 = Ym$, we have

$$\frac{E_{cm}^2}{m^2} = X^2 + Y^2 - 2g_{\mu\nu} u_1^{\mu} u_2^{\nu}. \tag{30}$$

Subsequently, we examine the collision between particles with equal masses $m_1 = m_2 = m$ ($X = Y = 1$) and initial energies $E_1 = E_2 = m$. We also explore the acceleration of magnetized particles near a magnetized BBMB black hole by employing the conventional equation for the textcolorred-CME of two colliding particles with equal masses. Consequently, the expression for the textcolorredCME is derived:

$$\mathcal{E}_{\rm cm}^2 = \frac{E_{\rm cm}^2}{2m^2} = 1 - g_{\alpha\beta} u_1^{\alpha} u_2^{\beta}. \tag{31}$$

To simplify calculations, we use the assumption that both particles possess identical mass ($m_1 = m_2 = m_0$) and equal energy ($\mathcal{E}_1 = \mathcal{E}_2 = 1$) while they are at an infinite distance from each other. This assumption allows for a focus on the intrinsic properties of the collision process while eliminating the complications that arise from different starting circumstances. We can formulate the expressions and conditions for the CME using the parameters provided. This derivation includes examining the collective impact of the particles' rest mass and kinetic energy as they approach and interact with the gravitational field of the BBMB black hole. This study aims to understand the potential outcomes of high-energy collisions and the subsequent formation of new particles in this extreme BH environment. Hence, by using Eqs. (17) and (21), the final representation for the collision energy in the center of the mass frame can be derived as stated in Refs. [72] as

$$\begin{aligned}\mathcal{E}_{cm}^2 = 1 &+ \frac{1}{\left(1 + g_s \Phi(r) + \beta\sqrt{f(r)}\right)^2}\left[\frac{\mathcal{E}_1 \mathcal{E}_2}{f(r)} - \frac{\mathcal{L}_1 \mathcal{L}_2}{r^2 \sin^2\theta_0}\right] \\ &- \frac{1}{f(r)}\sqrt{\mathcal{E}_1^2 - f(r)\left[(1 + g_s\Phi(r))^2\left(1 - \beta\sqrt{f(r)}\right)^2 + \frac{\mathcal{L}_1^2}{r^2\sin^2\theta_0}\right]} \\ &\times\sqrt{\mathcal{E}_2^2 - f(r)\left[(1 + g_s\Phi(r))^2\left(1 - \beta\sqrt{f(r)}\right)^2 + \frac{\mathcal{L}_2^2}{r^2\sin^2\theta_0}\right]},\end{aligned} \tag{32}$$

Below, we analyze CME in the equatorial plane. It is worth noting that the CME measures the total energy available in the center-of-mass frame of two colliding particles at the equatorial plane $\theta_0 = \pi/2$. In astrophysical scenarios, an enhanced CME near a black hole can be a mechanism for high-energy particle acceleration, which may convert to:

- the production of ultra-high-energy cosmic rays;
- energy extraction mechanisms such as the BSW process;
- the generation of high-energy radiation detectable in active galactic nuclei (AGN) or gamma-ray bursts.

In the context of BBMB black holes, the interplay between the conformal scalar field and magnetic interactions modifies the dynamics of charged and magnetized particles, leading to unique CME signatures.

Figure 6 illustrates the radial dependence of the CME $E_{\rm cm}$ for magnetized particle collisions in the background of a BBMB black hole. The figure explores how variations in the magnetic dipole interaction parameter β and the scalar coupling parameter g_s influence the energy release in high-energy collisions near the black hole. The top panel of the figure shows how the CME depends on the radial coordinate r/M for different values of the magnetic dipole interaction parameter, β, while keeping the conformal scalar coupling g_s fixed at $g_s = 0.2$. The results indicate that increasing β increases the CME at a smaller distance because the Lorentz force exerted by the external magnetic field modifies the effective potential, allowing for more energetic collisions in the near-horizon region. For the case of $\beta = 0$, which has no magnetic field, the CME follows a standard behavior in BBMB without magnetic interactions, peaking just outside the event horizon. As β increases, the CME grows more pronounced near $r \approx 2M$, suggesting that magnetic interactions can facilitate energy extraction and particle acceleration. The trend aligns with previous studies showing that external mag-

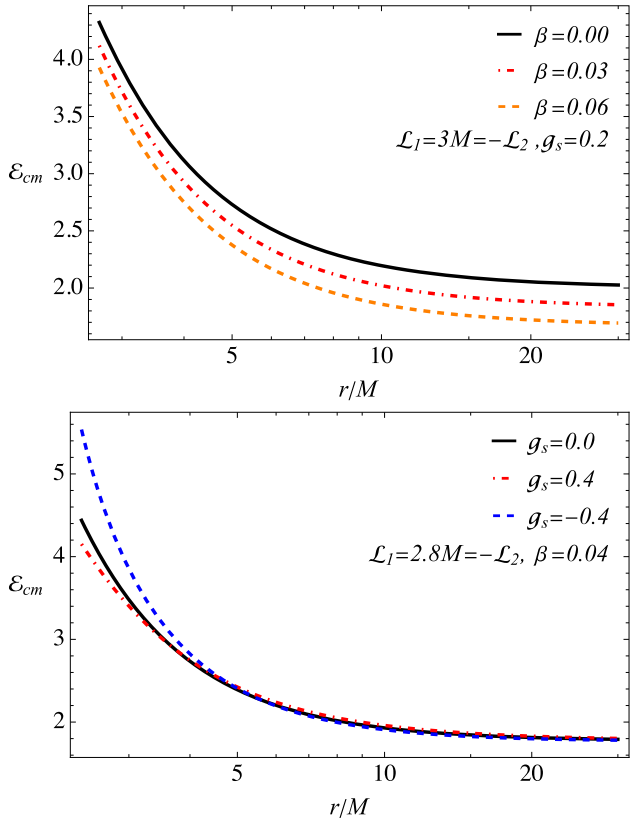

Fig. 6 Radial dependence of CME for different values of β (top panels) and g_s (bottom panels)

netic fields can amplify the efficiency of high-energy collisions in black hole spacetimes.

The bottom panel examines the influence of the scalar coupling parameter g_s on the CME for a fixed magnetic dipole parameter $\beta = 0.04$, for $g_s = -0.4$ negative scalar interaction, $g_s = 0.0$ zero scalar interaction and $g_s = 0.4$ positive scalar interaction. When $g_s < 0$, the CME is lower at all distances, implying that a repulsive scalar field weakens the binding energy of the system, making collisions less energetic. In the zero scalar field interaction case $g_s = 0$, the CME follows the standard BBMB black hole behavior, acting as a baseline case. Once we have positive (attractive) scalar field interaction $g_s > 0$, the CME increases significantly, particularly at smaller distances, suggesting that a strong, attractive scalar field enhances the energy of the possible collisions. The enhancement in CME due to positive g_s arises because the scalar field strengthens the gravitational attraction, forcing particles into tighter orbits and increasing their relative velocities before collision.

The CME increases with both the magnetic dipole interaction β and the scalar coupling g_s interactions, indicating that both factors contribute to amplifying collision energies. Magnetic interactions (modeled by β) primarily affect the CME in the near-horizon region, where the Lorentz force is strongest. Scalar interactions (modeled by g_s) modify the CME over a broader radial range, with attractive scalar fields enhancing collision energies and reducing repulsive fields. The interplay between gravitational, magnetic, and scalar field effects could provide observational signatures distinguishing BBMB black holes from standard Schwarzschild black holes.

These findings significantly affect the study of energetic astrophysical processes, such as black hole accretion dynamics, jet formation, and gamma-ray burst mechanisms.

6 Conclusion

In this work, we studied the dynamics of magnetized particles in the magnetized BBMB black hole spacetime, incorporating an external magnetic field and a conformally coupled scalar field. We derived the governing equations of motion and analyzed how the scalar coupling parameter (g_s) and the magnetic dipole interaction parameter (β) influence particle trajectories. Our results show that magnetic and scalar interactions introduce significant modifications to the effective potential, altering the stability conditions of circular orbits. Compared to the Schwarzschild case, the presence of a conformal scalar field creates a stronger gravitational pull, shifting the locations of stable orbits and changing the behavior of test particle dynamics. These modifications impact particle motion around compact objects, influencing accretion disk formation and energy transport in astrophysical settings.

We also analyzed the circular orbits of magnetized particles and determined the ISCO as a function of the parameters g_s and β. Our findings indicate that increasing g_s results in a smaller ISCO radius, as the attractive nature of the scalar field enhances gravitational binding. Conversely, larger values of β tend to shift the ISCO outward since the interaction between the particle's magnetic dipole moment and the external magnetic field generates an additional repulsive effect. Notably, in the limit of strong magnetic interaction, the ISCO can extend well beyond its Schwarzschild counterpart. These results highlight the interplay between gravitational, magnetic, and scalar fields effects in modifying orbital structures around black holes, which could have observational implications for astrophysical accretion disks.

In addition we examined the critical angular momentum ($\mathcal{L}_{cr}$) necessary for maintaining stable orbits. In the Schwarzschild case, the photon sphere at $r = 3M$ corresponds to $\mathcal{L}_{cr} = 4M$, but in BBMB spacetime, the presence of the scalar field and magnetic interaction shifts these thresholds. Our results show that for positive scalar coupling ($g_s > 0$), the effective gravitational attraction increases, reducing $\mathcal{L}_{cr}$ and allowing orbits to remain stable at lower angular momentum values. However, the external magnetic field introduces a repulsive force that counteracts this effect,

requiring a higher $\mathcal{L}_{cr}$ for stability. These findings suggest that magnetic and scalar fields interactions significantly alter the conditions for stable motion, influencing astrophysical phenomena such as jet formation and plasma dynamics around black holes.

A major outcome of our study is the impact of magnetic and scalar interactions on high-energy collisions. We computed the CME of colliding particles and found that both stronger magnetic fields (β) and scalar fields (g_s) enhance CME values. In particular, a combination of a strong attractive scalar field and an external magnetic field leads to an extreme amplification of CME, potentially reaching arbitrarily high values under fine-tuned conditions. This suggests that BBMB black holes could act as efficient particle accelerators, producing ultrarelativistic collisions in astrophysical environments. These effects may contribute to the formation of high-energy cosmic rays, gamma-ray bursts, and energetic outflows in black hole systems.

Our results demonstrate that the interplay between magnetic and scalar interactions fundamentally alters the behavior of particles in BBMB spacetimes, influencing both orbital stability and collision energetics. These modifications could have significant observational consequences in accretion disk structures, black hole jet dynamics, and astrophysical transients. Future studies should explore how these effects manifest in realistic astrophysical scenarios, including magnetized plasma dynamics and gravitational wave signatures from extreme particle interactions. Additionally, extending this analysis to rotating black holes and higher-dimensional gravity theories could provide deeper insights into the role of fundamental fields in extreme gravitational environments.

Acknowledgements BA and AHB would like to express their gratitude to the Dean of Research at King Fahd University of Petroleum and Minerals for approving the inbound visit of B. Ahmedov to the Mathematics Department, which contributed to the completion of a part of this research. J.R. thanks the grant No. F-FA-2021-510 of the Ministry of Higher Education, Science and Innovations of the Republic of Uzbekistan.

Data Availability Statement This manuscript has no associated data. [Authors' comment: Data sharing does not apply to this article, as no datasets were generated or analyzed during the current study.]

Code Availability Statement This manuscript has no associated code/software. [Authors' comment: Code/Software sharing does not apply to this article, as no code/software was generated or analyzed during the current study.]

Funded by SCOAP[3].

References

1. N.M. Bocharova, K.A. Bronnikov, V.N. Melnikov, Vestnik Moskovskogo Universiteta, Fizika, Astronomiia **6** (1970)
2. J.D. Bekenstein, Ann. Phys. **82**, 535 (1974). https://doi.org/10.1016/0003-4916(74)90124-9
3. K.A. Bronnikov, J.C. Fabris, Phys. Rev. Lett. **96**, 251101 (2006). https://doi.org/10.1103/PhysRevLett.96.251101. arXiv:gr-qc/0511109
4. Y.S. Myung, D.-C. Zou, Eur. Phys. J. C **79**, 641 (2019). https://doi.org/10.1140/epjc/s10052-019-7176-7. arXiv:1904.09864 [gr-qc]
5. B. Turimov, S. Usanov, Y. Khamroev, Phys. Dark Univ. **48**, 101876 (2025). https://doi.org/10.1016/j.dark.2025.101876. arXiv:2502.11185 [gr-qc]
6. F. Cocchiararo, A. Franchini, A. Lupi, A. Sesana, Astron. Astrophys. **691**, A250 (2024). https://doi.org/10.1051/0004-6361/202449598. arXiv:2402.05175 [astro-ph.HE]
7. Y. Wu, H. Feng, W.-Q. Chen, Eur. Phys. J. C **84**, 1075 (2024). https://doi.org/10.1140/epjc/s10052-024-13454-6. arXiv:2410.14113 [gr-qc]
8. D. Senjaya, Eur. Phys. J. C **84**, 607 (2024). https://doi.org/10.1140/epjc/s10052-024-12957-6
9. S.-W. Wei, Y.-X. Liu, Eur. Phys. J. Plus **136**, 436 (2021). https://doi.org/10.1140/epjp/s13360-021-01398-9
10. R. Kumar, S.U. Islam, S.G. Ghosh, Eur. Phys. J. C **80**, 1128 (2020). https://doi.org/10.1140/epjc/s10052-020-08606-3. arXiv:2004.12970 [gr-qc]
11. M. Astorino, Phys. Rev. D **95**, 064007 (2017). https://doi.org/10.1103/PhysRevD.95.064007. arXiv:1612.04387 [gr-qc]
12. M. Astorino, Phys. Rev. D **88**, 104027 (2013). https://doi.org/10.1103/PhysRevD.88.104027. arXiv:1307.4021 [gr-qc]
13. B. Turimov, A. Davlataliev, Y. Usmanov, S. Karshiboev, P. Tadjimuratov, Eur. Phys. J. C **84**, 1098 (2024). https://doi.org/10.1140/epjc/s10052-024-13426-w
14. B. Turimov, O. Rahimov, A. Davlataliev, P. Tadjimuratov, M. Norkobilov, S. Rahimova, Phys. Dark Universe **48**, 101855 (2025). https://doi.org/10.1016/j.dark.2025.101855. arXiv:2502.11210 [gr-qc]
15. K.D. Kokkotas, B.G. Schmidt, Living Rev. Relativ. **2**, 2 (1999). https://doi.org/10.12942/lrr-1999-2
16. J.L. Jaramillo, R.P. Macedo, L.A. Sheikh, Phys. Rev. Lett. **128**, 211102 (2022). https://doi.org/10.1103/PhysRevLett.128.211102. arXiv:2105.03451 [gr-qc]
17. S. Bahamonde, K.F. Dialektopoulos, C. Escamilla-Rivera, G. Farrugia, V. Gakis, M. Hendry, M. Hohmann, J. Levi Said, J. Mifsud, and E. Di Valentino, Rep. Prog. Phys. **86**, 026901 (2023). https://doi.org/10.1088/1361-6633/ac9cef. arXiv:2106.13793 [gr-qc]
18. J.A. Petterson, Phys. Rev. D **10**, 3166 (1974). https://doi.org/10.1103/PhysRevD.10.3166
19. F. de Felice, F. Sorge, Class. Quantum Gravity **20**, 469 (2003). https://doi.org/10.1088/0264-9381/20/3/306
20. F. Abdulxamidov, J. Rayimbaev, A. Abdujabbarov, Z. Stuchlík, Phys. Rev. D **108**, 044030 (2023). https://doi.org/10.1103/PhysRevD.108.044030
21. R. Penrose, Riv. Nuovo Cim. **1**, 252 (1969). https://doi.org/10.1023/A:1016578408204

22. M. Banados, J. Silk, S.M. West, Phys. Rev. Lett. **103**, 111102 (2009). https://doi.org/10.1103/PhysRevLett.103.111102. arXiv:0909.0169 [hep-ph]
23. T. Piran, J. Shaham, Phys. Rev. D **16**, 1615 (1977). https://doi.org/10.1103/PhysRevD.16.1615
24. J.D. Schnittman, Gen. Relativ. Gravit. **50**, 77 (2018). https://doi.org/10.1007/s10714-018-2373-5. arXiv:1910.02800 [astro-ph.HE]
25. R.D. Blandford, R.L. Znajek, Mon. Not. R. Astron. Soc. **179**, 433 (1977). https://doi.org/10.1093/mnras/179.3.433
26. S.U. Khan, Z.-M. Chen, Eur. Phys. J. C **83**, 704 (2023). https://doi.org/10.1140/epjc/s10052-023-11897-x
27. M. Bejger, T. Piran, M. Abramowicz, F. Håkanson, Phys. Rev. Lett. **109**, 121101 (2012). https://doi.org/10.1103/PhysRevLett.109.121101
28. E. Leiderschneider, T. Piran, Phys. Rev. D **93**, 043015 (2016). https://doi.org/10.1103/PhysRevD.93.043015. arXiv:1510.06764 [gr-qc]
29. F. de Felice, F. Sorge, S. Zilio, Class. Quantum Gravity **21**, 961 (2004). https://doi.org/10.1088/0264-9381/21/4/016
30. U. Uktamov, M. Fathi, J. Rayimbaev, A. Abdujabbarov, Phys. Rev. D **110**, 084084 (2024). https://doi.org/10.1103/PhysRevD.110.084084. arXiv:2406.03371 [gr-qc]
31. S.U. Khan, M. Shahzadi, J. Ren, Phys. Dark Univ. **26**, 100331 (2019). https://doi.org/10.1016/j.dark.2019.100331. arXiv:2005.09415 [gr-qc]
32. W.E. East, F. Pretorius, Phys. Rev. Lett. **110**, 101101 (2013). https://doi.org/10.1103/PhysRevLett.110.101101
33. W. Javed, M.B. Khadim, A. Övgün, Eur. Phys. J. Plus **135**, 595 (2020). https://doi.org/10.1140/epjp/s13360-020-00619-x. arXiv:2007.14844 [gr-qc]
34. J.D. Schnittman, Gen. Relativ. Gravit. **50**, 77 (2018). https://doi.org/10.1007/s10714-018-2373-5. arXiv:1910.02800 [astro-ph.HE]
35. B. Turimov, S. Hayitov, arXiv e-prints (2023). https://doi.org/10.48550/arXiv.2307.01919. arXiv:2307.01919 [gr-qc]
36. S. Kutlimuratov, N. Otojanova, I. Tadjibaev, K. Tillaboev, EUREKA: Phys. Eng. **4**, 3 (2024). https://doi.org/10.21303/2461-4262.2024.003416
37. M. Sharif, N. Haider, Astrophys. Space Sci. **346**, 111 (2013). https://doi.org/10.1007/s10509-013-1424-3. arXiv:1308.1116 [physics.gen-ph]
38. S.S. Kutlimuratov, N.B. Otojanova, I.U. Tadjibaev, Ukrain. J. Phys. **69**, 367 (2024). https://doi.org/10.15407/ujpe69.6.367
39. B. Narzilloev, A. Abdujabbarov, C. Bambi, B. Ahmedov, Phys. Rev. D **99**, 104009 (2019). https://doi.org/10.1103/PhysRevD.99.104009. arXiv:1902.03414 [gr-qc]
40. M. Zahid, O. Yunusov, C. Shen, J. Rayimbaev, S. Muminov, Phys. Dark Univ. **47**, 101734 (2025). https://doi.org/10.1016/j.dark.2024.101734
41. S.U. Khan, Z.-M. Chen, Chin. J. Phys. **92**, 1659 (2024). https://doi.org/10.1016/j.cjph.2024.11.001
42. R.K. Williams, Phys. Rev. D **51**, 5387 (1995). https://doi.org/10.1103/PhysRevD.51.5387
43. Z. Stuchlík, M. Kološ, A. Tursunov, Universe **7**, 416 (2021). https://doi.org/10.3390/universe7110416
44. V. Patel, K. Acharya, P. Bambhaniya, P.S. Joshi, Universe **8**, 571 (2022). https://doi.org/10.3390/universe8110571. arXiv:2206.00428 [gr-qc]
45. K.-I. Nakao, H. Okawa, K.-I. Maeda, PTEP **2018**, 013E01 (2018). https://doi.org/10.1093/ptep/ptx170. arXiv:1708.04003 [gr-qc]
46. M. Alloqulov, B. Narzilloev, I. Hussain, A. Abdujabbarov, B. Ahmedov, Chin. J. Phys. **85**, 302 (2023). https://doi.org/10.1016/j.cjph.2023.07.005
47. W. Yao, S. Chen, C. Liu, J. Jing, Eur. Phys. J. C **72**, 1898 (2012). https://doi.org/10.1140/epjc/s10052-012-1898-0. arXiv:1105.6156 [gr-qc]
48. G. Preti, Phys. Rev. D **70**, 024012 (2004). https://doi.org/10.1103/PhysRevD.70.024012
49. J.R. Rayimbaev, Astrophys. Space Sci. **361**, 288 (2016). https://doi.org/10.1007/s10509-016-2879-9
50. B. Narzilloev, J. Rayimbaev, A. Abdujabbarov, B. Ahmedov, C. Bambi, Eur. Phys. J. C **81**, 269 (2021). https://doi.org/10.1140/epjc/s10052-021-09074-z. arXiv:2103.11090 [gr-qc]
51. J. Rayimbaev, A. Abdujabbarov, M. Jamil, W.-B. Han, Nucl. Phys. B **966**, 115364 (2021). https://doi.org/10.1016/j.nuclphysb.2021.115364. arXiv:2009.04898 [gr-qc]
52. J. Rayimbaev, A. Demyanova, U. Camci, A. Abdujabbarov, B. Ahmedov, Int. J. Mod. Phys. D **30**, 2150019 (2021). https://doi.org/10.1142/S021827182150019X
53. J. Rayimbaev, A. Abdujabbarov, M. Jamil, B. Ahmedov, W.-B. Han, Phys. Rev. D **102**, 084016 (2020). https://doi.org/10.1103/PhysRevD.102.084016
54. N. Juraeva, J. Rayimbaev, A. Abdujabbarov, B. Ahmedov, S. Palvanov, Eur. Phys. J. C **81**, 124078 (2021). https://doi.org/10.1140/epjc/s10052-021-08876-5
55. J. Vrba, A. Abdujabbarov, M. Kološ, B. Ahmedov, Z. Stuchlík, J. Rayimbaev, Phys. Rev. D **101**, 124039 (2020). https://doi.org/10.1103/PhysRevD.101.124039
56. A. Abdujabbarov, J. Rayimbaev, F. Atamurotov, B. Ahmedov, Galaxies **8**, 76 (2020). https://doi.org/10.3390/galaxies8040076
57. A.H. Bokhari, J. Rayimbaev, B. Ahmedov, Phys. Rev. D **102**, 124078 (2020). https://doi.org/10.1103/PhysRevD.102.124078
58. S. Murodov, J. Rayimbaev, B. Ahmedov, A. Hakimov, Symmetry **15**, 2084 (2023). https://doi.org/10.3390/sym15112084. arXiv:2310.08046 [gr-qc]
59. J.M. Ladino, C.A. Benavides-Gallego, E. Larrañaga, J. Rayimbaev, F. Abdulxamidov, Eur. Phys. J. C **83**, 989 (2023). https://doi.org/10.1140/epjc/s10052-023-12187-2. arXiv:2305.15350 [gr-qc]
60. J. Rayimbaev, A. Abdujabbarov, D. Bardiev, B. Ahmedov, M. Abdullaev, Eur. Phys. J. Plus **138**, 358 (2023). https://doi.org/10.1140/epjp/s13360-023-03979-2
61. J.M. Bardeen, W.H. Press, S.A. Teukolsky, Astrophys. J. **178**, 347 (1972). https://doi.org/10.1086/151796
62. J. Rayimbaev, B. Ahmedov, M. Zahid, Eur. Phys. J. C **84**, 298 (2024). https://doi.org/10.1140/epjc/s10052-024-12981-7
63. J. Healy, I. Ruchlin, C.O. Lousto, Y. Zlochower, Phys. Rev. D **94**, 104020 (2016). https://doi.org/10.1103/PhysRevD.94.104020. arXiv:1506.06153 [gr-qc]
64. J. Rayimbaev, B. Narzilloev, A. Abdujabbarov, B. Ahmedov, Galaxies **9**, 71 (2021). https://doi.org/10.3390/galaxies9040071
65. S.U. Khan, O. Abdurkhmonov, J. Rayimbaev, S. Ahmedov, Y. Turaev, S. Muminov, Eur. Phys. J. C **84**, 650 (2024). https://doi.org/10.1140/epjc/s10052-024-12997-y
66. R. Abbott, T.D. Abbott, S. Abraham, F. Acernese, K. Ackley, A. Adams, C. Adams, R.X. Adhikari, V.B. Adya, C. Affeldt, M. Agathos, K. Agatsuma, N. Aggarwal, O.D. Aguiar, L. Aiello, A. Ain, P. Ajith, S. Akcay, G. Allen, A. Allocca, P.A. Altin, A. Amato, S. Anand, A. Ananyeva, S.B. Anderson, W.G. Anderson, S.V. Angelova, S. Ansoldi, J.M. Antelis, S. Antier, S. Appert, K. Arai, M.C. Araya, J.S. Areeda, M. Arène, N. Arnaud, S.M. Aronson, K.G. Arun, Y. Asali, S. Ascenzi, G. Ashton, S.M. Aston, P. Astone, F. Aubin, P. Aufmuth, K. AultONeal, C. Austin, V. Avendano, S. Babak, F. Badaracco, M.K.M. Bader, S. Bae, A.M. Baer, S. Bagnasco, J. Baird, M. Ball, G. Ballardin, S.W. Ballmer, A. Bals, A. Balsamo, G. Baltus, S. Banagiri, D. Bankar, R.S. Bankar, J.C. Barayoga, C. Barbieri, B.C. Barish, D. Barker, P. Barneo, S. Barnum, F. Barone, B. Barr, L. Barsotti, M. Barsuglia, D. Barta, J. Bartlett, I. Bartos, R. Bassiri, A. Basti, M. Bawaj, J.C. Bayley, M. Bazzan, B.R. Becher, B. Bécsy, V.M. Bedakihale, M. Bejger, I.

Belahcene, D. Beniwal, M.G. Benjamin, T.F. Bennett, J.D. Bentley, F. Bergamin, B.K. Berger, G. Bergmann, S. Bernuzzi, C.P.L. Berry, D. Bersanetti, A. Bertolini, J. Betzwieser, R. Bhandare, A.V. Bhandari, D. Bhattacharjee, J. Bidler, I.A. Bilenko, G. Billingsley, R. Birney, O. Birnholtz, S. Biscans, M. Bischi, S. Biscoveanu, A. Bisht, M. Bitossi, M.A. Bizouard, J.K. Blackburn, J. Blackman, C.D. Blair, D.G. Blair, R.M. Blair, O. Blanch, F. Bobba, N. Bode, M. Boer, Y. Boetzel, G. Bogaert, M. Boldrini, F. Bondu, E. Bonilla, R. Bonnand, P. Booker, B.A. Boom, R. Bork, V. Boschi, S. Bose, V. Bossilkov, V. Boudart, Y. Bouffanais, A. Bozzi, C. Bradaschia, P.R. Brady, A. Bramley, M. Branchesi, J.E. Brau, M. Breschi, T. Briant, J.H. Briggs, F. Brighenti, A. Brillet, M. Brinkmann, P. Brockill, A.F. Brooks, J. Brooks, D.D. Brown, S. Brunett, G. Bruno, R. Bruntz, A. Buikema, T. Bulik, H.J. Bulten, A. Buonanno, R. Buscicchio, D. Buskulic, R.L. Byer, M. Cabero, L. Cadonati, M. Caesar, G. Cagnoli, C. Cahillane, J. Calderón Bustillo, J.D. Callaghan, T.A. Callister, E. Calloni, J.B. Camp, M. Canepa, K.C. Cannon, H. Cao, J. Cao, G. Carapella, F. Carbognani, M.F. Carney, M. Carpinelli, G. Carullo, T.L. Carver, J. Casanueva Diaz, C. Casentini, S. Caudill, M. Cavaglià, F. Cavalier, R. Cavalieri, G. Cella, P. Cerdá-Durán, E. Cesarini, W. Chaibi, K. Chakravarti, C.L. Chan, C. Chan, K. Chandra, P. Chanial, S. Chao, P. Charlton, E.A. Chase, Phys. Rev. X **11**, 021053 (2021). https://doi.org/10.1103/PhysRevX.11.021053. arXiv:2010.14527 [gr-qc]

67. C.W. Bauer, Z. Davoudi, A.B. Balantekin, T. Bhattacharya, M. Carena, W.A. de Jong, P. Draper, A. El-Khadra, N. Gemelke, M. Hanada, D. Kharzeev, H. Lamm, Y.-Y. Li, J. Liu, M. Lukin, Y. Meurice, C. Monroe, B. Nachman, G. Pagano, J. Preskill, E. Rinaldi, A. Roggero, D.I. Santiago, M.J. Savage, I. Siddiqi, G. Siopsis, D. Van Zanten, N. Wiebe, Y. Yamauchi, K. Yeter-Aydeniz, S. Zorzetti, PRX Quantum **4**, 027001 (2023). https://doi.org/10.1103/PRXQuantum.4.027001. arXiv:2204.03381 [quant-ph]
68. S. Shaymatov, M. Alloqulov, B. Ahmedov, A. Wang, Phys. Rev. D **110**, 044005 (2024). https://doi.org/10.1103/PhysRevD.110.044005. arXiv:2307.03012 [gr-qc]
69. S. Jumaniyozov, S.U. Khan, J. Rayimbaev, A. Abdujabbarov, B. Ahmedov, Eur. Phys. J. C **84**, 291 (2024). https://doi.org/10.1140/epjc/s10052-024-12605-z
70. S. Murodov, J. Rayimbaev, B. Ahmedov, A. Hakimov, Symmetry **15**, 2084 (2023). https://doi.org/10.3390/sym15112084. arXiv:2310.08046 [gr-qc]
71. M. Zahid, S.U. Khan, J. Ren, Chin. J. Phys. **72**, 575 (2021). https://doi.org/10.1016/j.cjph.2021.05.003. arXiv:2101.07673 [gr-qc]
72. E. Hackmann, H. Nandan, P. Sheoran, Phys. Lett. B **810**, 135850 (2020). https://doi.org/10.1016/j.physletb.2020.135850. arXiv:2006.05045 [gr-qc]